CrystEngComm

RSC Publishing

PAPER

View Article Online
View Journal | View Issue

Bulk AlN single crystal growth on foreign substrate and preparation of free-standing native seeds

Cite this: *CrystEngComm*, 2013, **15**, 2232

R. Radhakrishnan Sumathi*

Physical vapour transport growth of aluminium nitride (AlN) single crystals on silicon carbide (SiC) substrates has been optimised and crack-free, large-area, free-standing (0001) AlN wafers were prepared from the grown template crystals. 28 mm diameter single crystals without any polycrystalline surroundings were obtained. Different off-oriented substrates give rise to different growth modes. Sharp and symmetric line shapes of X-ray diffraction (XRD) rocking curves and high intense Raman phonon mode peaks prove high structural quality and homogeneity of the grown crystals. Full width at half maximum of the rocking curves is 72 arcsec for symmetric 00.2 reflection and 200 arcsec for asymmetric 10.3 reflection, representing a low screw as well as edge type threading dislocations. Wet chemical etching results also confirm the above XRD results and the estimated etch pit density is as low as 2–5 $\times$ 10^5 cm^{-2}. The growth surfaces of all the crystals show only Al-polarity as inferred by the etching analysis. The concentration of silicon and carbon impurities incorporated from the SiC substrate decreases with the growth length of the AlN crystals. These impurities might play a decisive role in determining the optical properties of the crystal and be responsible for the absence of near-bandgap excitonic luminescence. Confocal Raman spectra show only the phonon modes allowed by the selection rules for the measured symmetry. The observed E_2(high) phonon mode frequency very closely matches the reported stress-free phonon frequency of AlN. This work demonstrates that AlN templates prepared on SiC as a foreign substrate can be used as native seeds for the growth of further homo-epitaxial layers and crystalline boules.

Received 1st October 2012,
Accepted 7th November 2012

DOI: 10.1039/c2ce26599k

www.rsc.org/crystengcomm

1 Introduction

The superior physical and chemical properties of AlN, such as ultra-wide direct bandgap,[1,2] high melting point,[3] high thermal conductivity,[4] high resistivity, high breakdown field, high thermal and good chemical stability, good mechanical strength, radiation hardness and miscibility with gallium nitride (GaN) in the entire alloy region[5] make it technologically important. Solid-state optoelectronic devices such as light-emitting diodes (LEDs) and laser diodes (LDs) based on III-nitride materials, emitting in the ultraviolet (UV) spectral range are of great interest for various applications. These include water purification, sensors, bio-agent detection systems, medical diagnosis devices, UV curing and material processing. Especially efficient, high-power mid-UV LEDs, which emit in the 240–280 nm range, have the potential to replace mercury lamps presently used in water and air purification applications. However, this potential has not yet been fully realized since output powers, efficiencies and lifetimes of these mid-UV LEDs have been limited by the high defect level in the device's active region. Typically, the mid-UV LEDs have been fabricated on AlN template layers that are again grown on sapphire as substrates due to the lack of readily available native substrates. These template layers had dislocation densities greater than 10^{10} cm^{-2}. Several strategies have been utilized to reduce the dislocation density (DD) in the active region of the LED device, including lateral overgrowth, thick template layers, and pulsed epitaxial growth. Even then, these methods were only successful in reducing the DD to the 10^8 cm^{-2} range.[6] This high DD limits both the efficiency and the reliability of devices grown on such layers.[7,8] An alternative and also possibly the best approach for reducing the DD is the use of a low defect AlN substrate.[9]

Currently, physical vapour transport (PVT – also known as the sublimation–recondensation method) is the most successful and widely used method for producing large area AlN native substrates. It is difficult to grow AlN by conventional melt growth or solution growth methods because of its extreme properties. The PVT method can be used to grow AlN with low dislocation densities at a reasonably high growth rate which makes it attractive for industrial productions. However, a significant decrease of optical transparency[10–12] is usually observed at photon energies below the bandgap, attributed to the presence of Al vacancies (V_{Al}), substitutional impurities (carbon, oxygen) and their complexes. Another method for preparing AlN with good optical properties is

Crystallography Section, Department of Earth and Environmental Sciences, Ludwig Maximilians University, D-80333 Munich, Germany. E-mail: sumathi@lrz.uni-muenchen.de

growing a thick AlN layer by hydride vapour phase epitaxy (HVPE) on foreign substrates such as SiC or sapphire and then separating the layer, although the growth rate is very low. A free-standing AlN substrate is usually obtained through removal of the back-substrate by cutting and optically polishing both sides. Substrates prepared by this method showing a steep optical transmission cut-off near the band edge have also been reported. But, owing to different lattice parameters and thermal expansion coefficients between AlN and the foreign substrates, generation of high densities of dislocations ($>10^7$ cm^{-2}) and cracks in the layer is a severe problem with this method. Therefore, use of AlN substrates prepared by the sublimation–recondensation method as starting seeds even for the HVPE method becomes one of the good choices in the preparation of free-standing AlN wafers having both deep-UV transparency and high crystalline quality.[13] We believe that the most economically effective way of producing AlN single crystalline wafers for any device applications is to develop reproducible processes for growing bulk single crystals and then do subsequent wafer slicing. This approach will have an advantage in the sense that the crystal can be sliced in various directions and so substrates with required orientations, including non-polar and semi-polar ones, could in fact be obtained. So the development of large-area AlN with PVT technique is of significant relevance particularly for UV devices.

As AlN does not exist by nature, different means of obtaining seeds for single crystal growth have to be looked at. These may include spontaneous nucleation, grain selection and further expansion and growth on readily available foreign substrates such as silicon, SiC and sapphire. The spontaneous nucleation yields crystals of highest structural perfection, but they are very small in size and limited in shape. Seeding on SiC substrate seems to be especially promising to rapidly obtain bulk AlN crystals of industrially-relevant dimensions. Though the lattice and thermal expansion mismatch properties favours the selection of SiC over the other materials, still the small difference in those physical properties are good enough to generate defects at the AlN–SiC interface and/or mosaicity present in the SiC seed might lead to formation/continuation of grain boundaries and tilted domains in AlN, which are undesirable when using such crystals as seeds for subsequent homoepitaxial growth. Hence, one of the main issues in the PVT growth of AlN is to optimise proper growth process conditions in order to yield crystals with reduced defects as mentioned above. The other issue is that the incorporation of unintentional impurities such as silicon, carbon, oxygen, into the grown crystals and controlling such contamination will be the key prerequisite. These two problems pose a stiff challenge and need to be solved quickly for any future development and commercialisation of AlN substrates prepared by this method. In this research study, we address one of the hindering issues namely the structural quality of the crystals in the hetero-epitaxial growth and attained remarkable improvement. Furthermore the grown material was also evaluated in the limelight of intrinsic defects/impurities combinations in respect to their optical properties, which makes a greater impact on deep-UV absorption in PVT grown bulk AlN.

2 Experimental

Bulk AlN single crystals were grown hetero-epitaxially on (0001) SiC substrates using PVT method with an inductively heated reactor. Different hexagonal polytypes (6H and 4H) and off-orientations (0°, 2° and 4° from (0001) plane, *i.e. c*-plane) of the substrate have been investigated. The crystals were grown in the temperature range of 1800–1900 °C in tantalum carbide (TaC) crucibles. The AlN source powder has been purified by sintering at high temperatures around 1900–2000 °C (above the growth temperature), to reduce the addition of oxygen and carbon impurities starting from the source itself. Pre-sintered AlN source powder sublimes from the bottom of the TaC crucible kept at a relatively higher temperature, and the crystal grows by recondensation on the SiC seed at the top of the crucible maintained at a relatively lower temperature. The system was pumped down to high vacuum and a constant flow of high-pure nitrogen was then introduced with a pressure of about 300–700 mbar as determined for the required growth rate. The corresponding source and seed temperatures were measured using two infrared optical pyrometers. The desired temperature gradient along the crucible was controlled by the position of the inductive coil relative to the crucible and a moderate growth rate of 20–40 μm h^{-1} has been achieved, taking in to consideration, the etching of the substrate by vigorous Al vapour.

In order to evaluate the crystalline quality and structural perfection of the grown crystals, high-resolution X-ray diffraction (HRXRD) and confocal Raman measurements were carried out. The ω-scan rocking curves (RC) were measured using a Phillips "X'pert epitaxy" instrument in double axis geometry using a Cu Kα_1 X-ray source with a four-bounce Ge[220] monochromator. The foot-print of the X-ray beam on the measured samples was approximately 1 × 2 mm^2. Additionally, the symmetry and unit cell parameters of the grown crystals were checked using an Oxford Gemini Ultra A diffractometer. An enhanced Mo Kα X-ray source with λ = 0.71073 Å was used in these measurements, and the beam collimator diameter was 0.1 mm. Confocal Raman measurements were carried out using a Labspec Xplora system with a 50× objective and 1800 mm^{-1} grating. The 532 nm laser was used for the excitation and the line positions were determined with a nominal spectral resolution of 1 cm^{-1} for the utilized grating. Surface morphology of the crystals was examined by optical as well as laser scanning microscopy (LSM). Wet chemical etching with KOH : NaOH eutectic melt was performed on the polished *c*-plane samples to analyse the polarity and defect density. In addition, cross-sectional samples were also prepared to investigate the incorporation of silicon (Si) and carbon (C) along the grown crystal length by electron probe microanalysis (EPMA). Optical properties of the crystals in terms of impurity-related below-bandgap transi-

tions were analysed by room temperature cathodoluminescence (CL) measurements. The CL measurements were performed using a scanning electron microscope attached with an UV-enhanced CCD camera/monochromator setup. The measurements were carried out with a nominal beam current of 130 nA at 20 kV acceleration voltage. It should be mentioned that all the measurements (if not mentioned specifically) were carried out on either as-grown or polished *c*-plane surfaces, prepared 3–5 mm away from the AlN–SiC hetero-interface. The mechanical polishing (using diamond paste up to the particle size of 0.25 μm) of the samples prepared from the crystals gives the RMS surface roughness of around 2–4 nm, which could be a sufficient surface finish for the measurements.

3 Results and discussion

3.1 Bulk AlN crystals, surface morphology and growth mode

During this study, different growth parameters such as temperature, N_2 pressure, temperature gradient, source purity, *etc.*, have been investigated and optimised. The grown AlN single crystals are of 28 mm in diameter and up to 8 mm in thickness. They are typically transparent-yellowish or amber in colour and exhibit excellent hexagonal morphology (Fig. 1a) including flat, well-pronounced *c*-facets (basal plane). The quality of the starting substrate is important to get a good AlN crystal. The micro-pipes (crystallographic defects) in the SiC substrate will affect the epitaxial growth by following through the growth direction of the crystals. Once they propagate into the growing AlN crystal, the crystal will then contain micro-holes. Even macro-holes may also be formed due to strong back evaporation at this defect site. This will be critical for further usefulness of these AlN crystals as native seeds or in epitaxial device fabrication. Two competing processes, namely growth of AlN and decomposition of the SiC substrate occur at the same time. If the AlN layer does not fully cover the SiC substrate before it is decomposed, this will lead to the formation of such holes. In our experiments, the growth has been performed at somewhat lower temperatures to mitigate the propagation of micro-pipes if any, as well as the back sublimation of both SiC and the growing crystal. Thus, the grown crystals do not have any macro- or micro-holes. The crack in the grown crystals, due to the difference in the thermal expansion coefficient mismatch between AlN and SiC, has also been eliminated under the applied process conditions. It may be pointed out here that AlN crystals grown on SiC should be at least 1.5–2 mm thick in order to avoid cracking during cool-down from the high growth temperature. One of the typical crack-free surfaces of a 3.5 mm thick AlN single crystal is shown in Fig. 1a. In all the grown crystals, the presence of well-developed, shiny $\{10\bar{1}n\}$ side facets (indicated by arrows in Fig. 1a) shows the high crystalline quality. Further the crystals are free from the polycrystalline rim and this is one of the reasons for the elimination of cracks and also for the formation of good facets. The reproducible and well-controlled growth process was achieved under the optimised conditions.

Three kinds of growth modes depending on the off-orientation of the SiC substrates were observed on the AlN crystals grown under the same process conditions. The growth morphology was not influenced by the substrate polytypes: 1) in the first case (as in Fig. 1a), the crystals have a single nucleation point at one edge of the crystal. A step-flow begins at this point and smoothly flows to the other end. This represents a 2D layer growth mechanism without any island formation. Usually this kind of continuous step-flow growth is observed when 4° off-oriented substrates were used. In addition, in such crystals, the single nucleation center is hexagonal in morphology with many spiral steps surrounding it. The optical microscopic picture of this nucleation center is shown in Fig. 1b. However, the high off-orientation additionally results in macro-step formation or step-bunching (Fig. 2a and c). Foreign particles and impurities deposited on the surface are possible causes of such a step bunching.[14] Further, it has been reported that during nitrogen doping in SiC crystal growth, the equidistant step trains can be transformed into meandering macro-steps by nitrogen adsorption on the growing crystal surface.[15] During this AlN growth on SiC substrates, even though there are no intentional dopants, Si and C impurities might play a dominant role in the formation of macro-steps. The silicon concentration of 1–2 wt% has been detected in the crystal surface by EPMA measurements. The carbon concentration could not be accurately measured by EPMA, nevertheless the semi-quantitative value of ~6 wt%

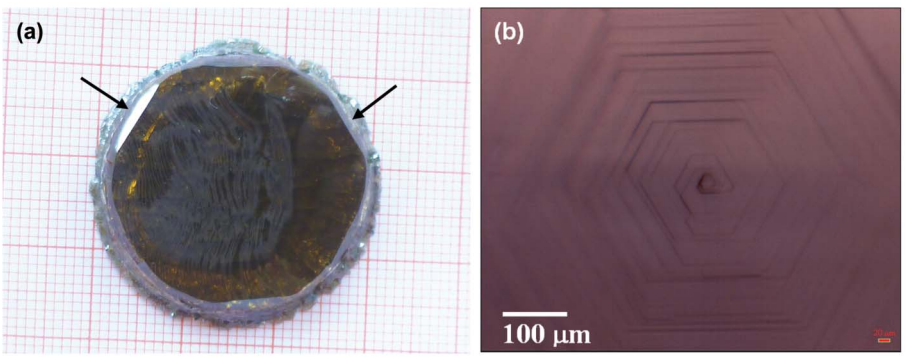

Fig. 1 (a) AlN single crystal grown on 4° off-oriented 4H–SiC substrate showing a crack-free surface and uniform step-flow growth; $\{10\bar{1}n\}$ side facets are indicated by arrows. (b) A single nucleation center on the flat surface, also exhibiting hexagonal morphology with spiral steps.

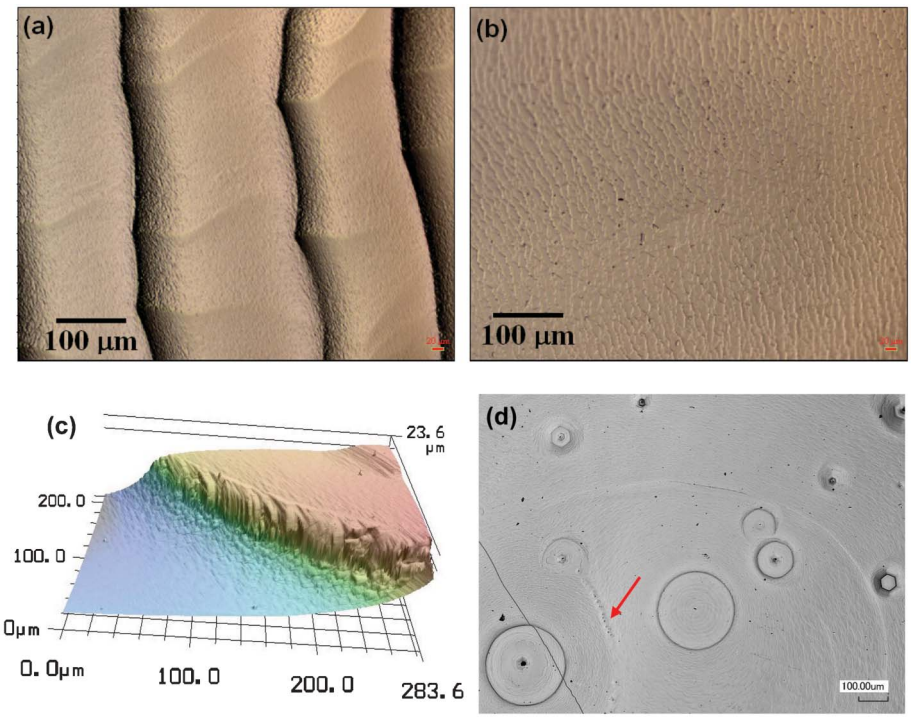

Fig. 2 (a) Macro-steps observed on the crystal surface, grown with off-oriented substrate. (b) Uniform characteristic step-flow on the flat region. (c) Step-bunching between the two terraces. (d) LSM picture showing the 3-dimensional multi-nucleation in the crystals grown on on-axis substrates.

could be estimated. The observed macro-steps are not very straight and they flow as wave with significantly varying spacing along the steps. These steps are greater than 20 μm in height with broad terraces of 100–200 μm width as displayed in Fig. 2a. But, very smooth steps were observed as shown in Fig. 2b, on the flat surface region (see right hand side of the Fig. 1a) and no inclusions were noticed microscopically.

2) Some of the crystals exhibit a single nucleation center at the middle of the surface and show growth morphology as if they have been growing as a single spiral. The steps starting from the growth spiral are flowing smoothly in all directions (not shown here). This kind of growth mode is normally observed while using slightly off-oriented (2°) substrates. The optimum vapour supersaturation of case-1 is relatively high for this case.[16] 3) If the on-axis (*i.e.* 0° off-orientation) substrates are used, the growth starts with multi-nucleation and the crystal surfaces are characteristic of many concentric rings with both circular and hexagonal morphology, suggesting a screw dislocation-mediated 3D island growth (Fig. 2d). On the other hand, some studies carried out on nitride[17] and other material systems[18] have reported that the concentric, closed ring structures correspond to edge dislocations. These concentric rings are of varying size (up to 200 μm) and height (up to 3 μm). There are also some grain boundaries formed in these crystals. The grain boundaries are decorated by small spirals on the as-grown surface and are clearly seen in the Fig. 2a as marked by an arrow. This growth mechanism suggests that the on-axis substrates may not be ideal for the growth of AlN by this method. Although in all the above three discussed cases most of the growth conditions were maintained almost identical, it should be mentioned that there might be always very slight changes in the temperature field due to continuous degradation of crucible/insulation/heating materials.

3.2 Structural quality

3.2.1 X-ray diffraction rocking curves. ω-scan rocking curve full width at half maximum (FWHM) values of symmetric 00.2 reflections of the grown crystals are usually around 100 arcsec. Some samples even show very narrow rocking curves with FWHM values less than 100 arcsec, indicating a very high crystalline quality of the grown crystals. Fig. 3a and b show HRXRD rocking curves of the symmetric 00.2 and asymmetric 10.3 reflections of the AlN crystals grown on various SiC substrates (on-axis 6H and 2° off-axis 4H). For both the samples shown here, the rocking curves for the symmetric 00.2 reflection are narrow with the FWHM values of 72 and 110 arcsec. The peaks are symmetric in shape, which indicates a uniform crystallographic tilt distribution of neighbouring subgrains and also reflects less mosaicity. The asymmetric 10.3 reflection of the samples gives slightly broad peaks with a FWHM of around 200 arcsec (by Gaussian fitting) showing a larger twist angle between the subgrains rather than the tilt angle. This indicates that the edge type dislocations, which primarily distort the asymmetric planes, are higher than the threading screw dislocations. Nevertheless, this value of 200 arcsec is fairly good since the creation of edge threading dislocations are generally more in the case of hetero-epitaxial growth. Additionally, these asymmetric curves exhibit a small shoulder to the left side of the main peak. This peak splitting

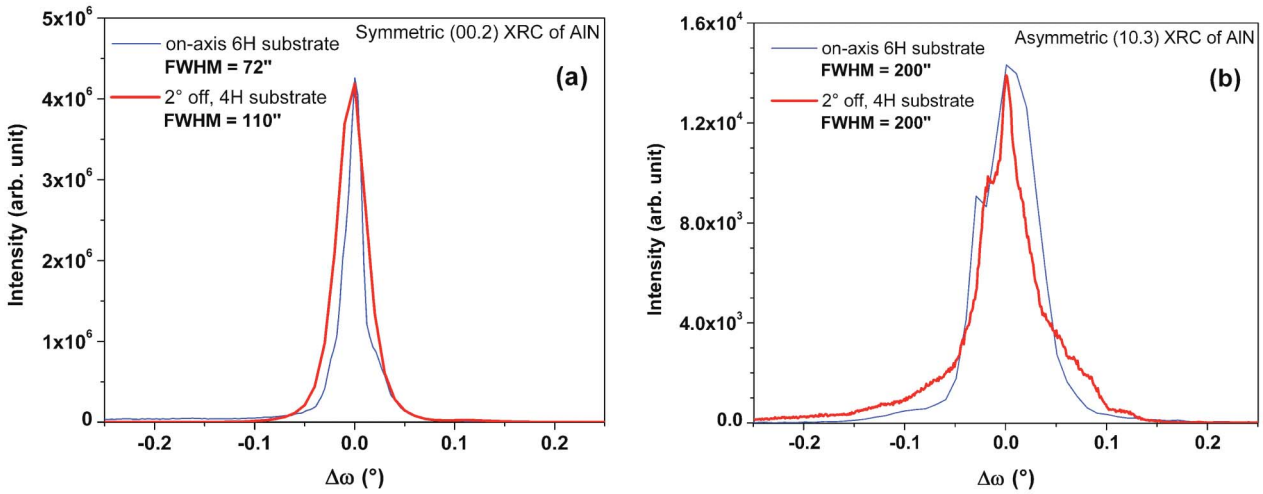

Fig. 3 X-ray diffraction rocking curves of AlN single crystals grown on different SiC substrates (a) symmetric 00.2 reflection (b) asymmetric 10.3 reflection.

implies the presence of low-angle grain boundaries (LAGBs). The symmetric (00.2) rocking curve measurements performed at different points over the surface of a 1-inch diameter template show no significant change in FWHM values and peak positions/intensities, indicating good structural homogeneity of the samples. The obtained FWHM values in this work are much lower than the already literature-reported values for AlN crystals grown on SiC substrates,[11,19,20] and are almost comparable with the homo-epitaxially grown crystals.[21,22]

The unit cell parameters were calculated for the crystals by measuring all possible reflections. The average value of the unit cell parameters, measured for this hetero-epitaxially grown AlN crystal on 2° off-oriented 4H–SiC substrate, are a = 3.110(17) Å and c = 4.985(13) Å which vary slightly (in the order of 10^{-3}) from the homo-epitaxially grown AlN crystals[13] (a = 3.1111 Å; c = 4.9808 Å). The slightly reduced "a" lattice constant implies a small compressive strain in the grown crystals and likewise, the increased "c" lattice parameter indicates that the layers have a tensile strain along the growth direction. Nonetheless, these values show a fairly less lattice deformation when considering the lattice mismatch between AlN (a = 3.1111 Å)[23] and 4H–SiC (a = 3.0730 Å)[24] under the established crystal growth conditions.

3.2.2 Confocal Raman measurements. Structural properties of the grown crystals were additionally evaluated by Raman spectroscopy in backscattering geometry with $Z(X,X)\bar{Z}$ polarisation. Fig. 4 shows a confocal Raman spectrum of an AlN single crystal grown on a 4° off-oriented 4H–SiC substrate. Only the phonon modes that are allowed by the selection rules for this symmetry (c-plane AlN) are seen in the spectrum. Their positions are: E_2(low) mode at 247.7 cm^{-1}, the E_2(high) mode at 656.9 cm^{-1} and the A_1(LO) mode at 890.9 cm^{-1}. These peaks are always present in all the crystals and the peak positions closely match with the unstrained, self-nucleated AlN crystal.[25] Particularly, the E_2(high) mode, which is considered to be the measure of the quality, is only 0.5 cm^{-1} shifted from the stress-free AlN value of 657.4 cm^{-1} and it also has a low FWHM value of 18 cm^{-1}. This small shift in peak position towards lower wavenumbers indicates the presence of a very low tensile stress or can even be described as nearly stress-free. As mentioned in the previous section, the slightly higher "c" lattice parameter value also supports this result. Further, there is no peak splitting of the E_2(high) mode, unlike what has been reported[26] for AlN grown on SiC due to some inclusions which give unallowed TO phonon modes.[27] It should also be mentioned that the measurements performed at different places on the as-grown surfaces also exhibit only the allowed LO phonon modes for this symmetry. This implies that the as-grown surface is very smooth and has no inclusions or holes (absence of TO modes). The E_2(high) FWHM value presented here is the lowest value reported for the hetero-epitaxially grown AlN crystal as far as we know. But when compared to self-nucleated,[28] nominally pure crystals, these obtained FWHM values of E_2(high) and A_1(LO) are larger,

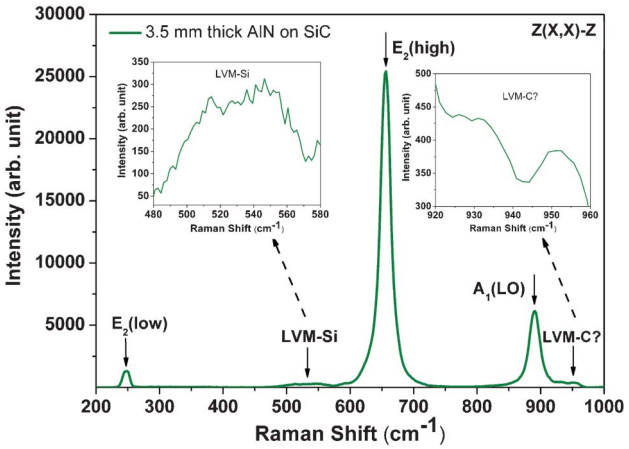

Fig. 4 Raman spectra of AlN single crystal grown on 4° off-axis 4H–SiC substrate, showing a narrow E_2(high) peak. Two inset graphs show the presence of silicon and carbon impurities.

indicating the considerable defect as well as impurity concentrations in the crystals.

There are two additional low-intensity broad bands observed in all the samples at around 480–580 cm^{-1} and 920–960 cm^{-1}. The enlarged view of these bands is shown as insets in Fig. 4. These weak features are presumably attributed to the local vibrational modes (LVMs) of silicon and carbon impurities respectively. These LVMs perturb the intrinsic crystal vibration, causing the asymmetric line shape of the LO phonon mode.[27] Furthermore, the presence of a high concentration of free-carriers of donor (in this case silicon) or acceptor (mainly carbon) impurities may strongly couple with the A_1(LO) phonon and can also affect the line shape symmetry.[29] This phonon–plasmon coupling may be one of the reasons why it is quiet difficult to obtain good conductivity in AlN. This could also be the reason for the observed line shift of the A_1(LO) mode by 1 cm^{-1} with respect to the reference value.[28] Nonetheless, these two impurities (*i.e.* Si and C) are unavoidable in this hetero-epitaxial growth due to the fact that they are unintentionally added into the growing crystal from the SiC substrate. But, their concentration reduces sharply with the distance while moving from the interface as seen by EPMA analyses[30] and further confirmed by the decreasing intensity of these broad LVM peaks with the grown length of the crystals.[16] Further efforts will have to be devoted to address one of these remaining issues with this hetero-epitaxial growth method so as to control and/or to reduce the incorporation of these two main impurities.

3.2.3 Wet chemical etching analysis. Defect-selective wet chemical etching of AlN has been carried out on the chemo-mechanically polished samples. Proper etching conditions were found out by varying the temperature, time as well as the KOH : NaOH eutectic ratio. The etching time and temperatures seem to be influenced by the impurity content of the samples. For revealing defects in AlN grown on SiC, the optimised time of etching is in the range of 120–150 s and a temperature of around 350 °C. Longer time or higher temperature etching resulted in over-etching of the samples and also merging of etch pits together. Etch pits were clearly revealed with the KOH : NaOH ratio of 1 : 1. Fig. 5 shows the optical microscopic images of typical etch features seen with the AlN samples grown on 2° off-oriented 4H–SiC substrates. The grown crystals always exhibit ''Al-polar'' growth surface independent of the substrate polytype. Moreover, ''N-polar'' inversion domains were not observed in the etched surfaces.

In Fig. 5a, the screw- (bigger pits), the edge- (smaller pits) and the mixed-type (medium pits) threading dislocations are distinguishable. As can be seen from Fig. 5b, the etch features consist of hexagonal idiomorphic etch pits as well as oval-shaped pits (as marked by an arrow). The symmetrical hexagonal pits are the typical etch pits revealing Al-polarity of the surface. The oval-shaped pits are asymmetrical in shape and have a long tail, implying that they are inclined with respect to the (0001) surface. They are attributed to basal plane dislocations (BPD), and these BPDs are the result of thermo-elastic stress. The density of BPDs is higher at the edge of the wafer indicating more thermo-elastic stress in the periphery of

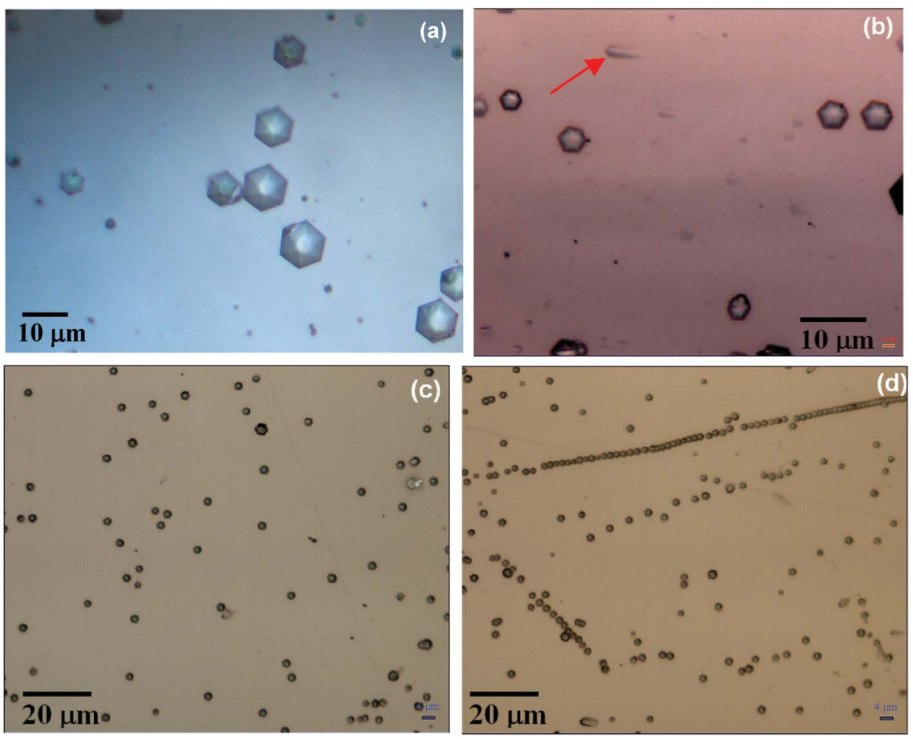

Fig. 5 Etch pits on the ''Al-polar'' growth surface of the AlN grown on a 2° off-axis SiC substrate. (a) Hexagonal etch pits showing screw (big pits) and edge (small pits) dislocations. (b) Picture of idiomorphic etch pits and oval-shaped basal plane dislocations marked by arrow. (c) Uniform distribution of etch pits. (d) A long dislocation line representing LAGB.

the crystal. This can be attributed to the radial temperature gradient inside the crucible.[31] The etching was also carried out on the wafers cut longitudinally from different lengths of the crystal (*i.e.* from the bottom to the top part) in order to understand the propagation of misfit-related dislocations. The samples from the near interface regions (*i.e.* 1 mm away from the interface) show a total etch pit density (EPD) in the order of 10^6 cm^{-2}, while the samples from the top part (*i.e.* 5 mm away from the interface) exhibit a reduced EPD in the range of 2–5 $\times$ 10^5 cm^{-2}. This shows that all the misfit-related dislocations are not propagated through the grown length due to strain relaxation and thus their densities are decreased. This is in good agreement with the XRD and Raman measurement results where the FWHM values reduce with the crystal length. Furthermore, within each sample (area 10 $\times$ 10 mm^2) at different positions (except the very edge), the EPD is in the same order of magnitude and shows the uniform distribution of defects (Fig. 5a–c). But in some instances, when the growth conditions are deviated from the normal optimised conditions (*i.e.* if there is an additional carbon incorporation from the growth environment, or non-uniform thermal fields because of insulation material degradation), low-angle grain boundaries were observed in the form of etch pit arrays/lines as shown in Fig. 5d. In addition, dislocation-bunching has also been observed in these crystals.

3.3 Optical properties of the grown AlN

Room temperature CL spectra measured on two different AlN crystals (plotted in a semi-logarithmic scale to show the weak features) are shown in Fig. 6a. The CL spectra of the samples mainly consist of two luminescence bands at around 1.9 eV and 3.4 eV. The intensity of the 3.4 eV (near-UV luminescence) band is almost two orders of magnitude higher than that of the 1.9 eV (visible luminescence) band, and having an FWHM of 290 meV. The CL spectra taken at different positions (Fig. 6b) of the same sample do not differ in their peak position and the peak width. The origin of this near-UV luminescence peak at 3.4 eV is not yet clear and is still being discussed in the literature. Some of the earlier reports[32] showed that the intensity of this band increases with the oxygen concentration, and it has been assigned to V_{Al}-oxygen related complexes. This CL band around 3.4 eV has also been observed for nominally pure, yellow-coloured AlN crystals with very low silicon and carbon concentrations,[33] and it has been attributed to a donor–acceptor pair transition involving a shallow donor and the isolated aluminium vacancies.[34,35] Interestingly, a similar peak has recently been reported for AlN crystals even with very high Si and C concentrations in the order of 10^{20} cm^{-3} and 10^{19} cm^{-3}, respectively.[36] In that report, it was seen that the 3.4 eV peak is observed only if the silicon is electrically active (*i.e.* if the crystal is weakly n-type) and this band was attributed to the donor–acceptor pair transition. The crystals in our study were also unintentionally doped to a high silicon and carbon concentration ($>10^{20}$ cm^{-3}) and show a luminescence band at 3.4 eV. It is not known whether the silicon in our crystals is electrically active or not, as the electrical measurements have not been done so far and we could not provide the supportive evidence to that argument from our crystals.

Also for the other broad luminescence peak at 1.9 eV, the origin is ambiguous and has not been investigated in much detail. Strassburg *et al.*[37] proposed that the nitrogen vacancies and Al interstitial point defects are responsible for the emission band around 2.0 eV. Further similar broad bands at this energy have been reported in the case of insulating AlN samples.[36] As already mentioned in section 1, the PVT grown AlN crystals do not show optical transmission in the deep UV region due to below-bandgap optical absorption related to impurities, particularly carbon. Further, such impurities can decrease excitonic lifetime and radiative recombination. Hence, there is no excitonic peak observed in CL spectra for

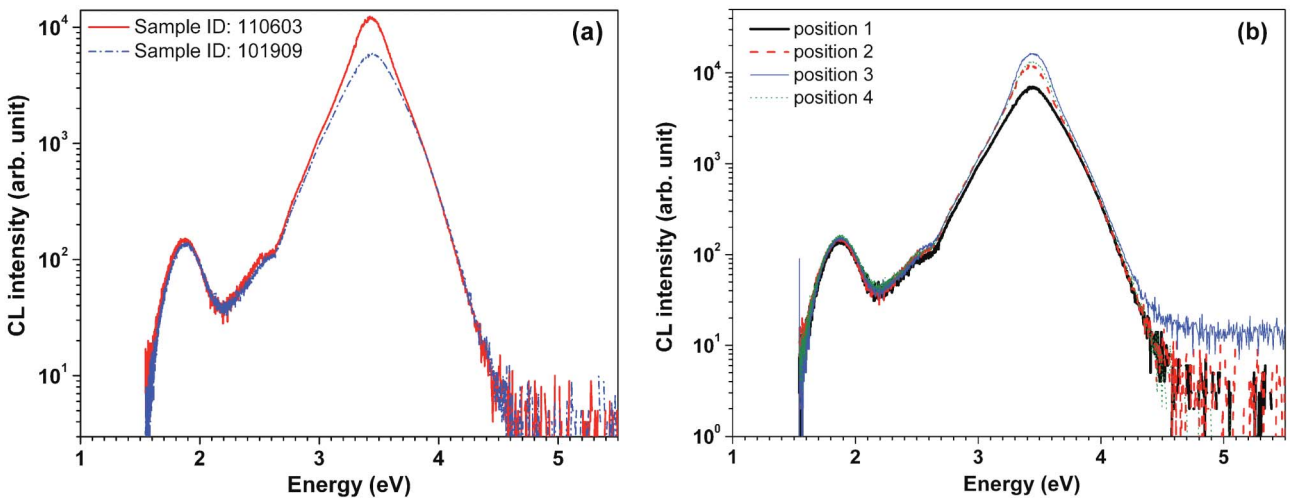

Fig. 6 Room temperature CL spectra – a semi-logarithmic scale is used to show the weak features (a) measured on two different AlN samples (b) various locations of the same sample showing constant peak positions.

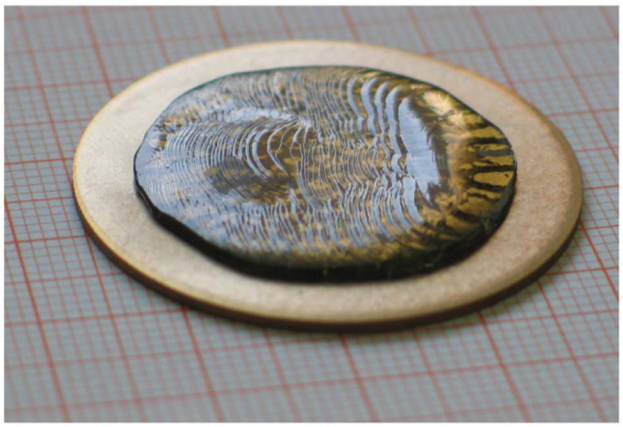

Fig. 7 Photograph of a free-standing AlN wafer – removed from the SiC substrate and attached to a seed holder for further homo-epitaxial growth. Diameter = 28 mm, thickness = 1.5 mm.

any of the investigated samples and also the bandgap of the grown crystals could not be found out.

3.4 Free-standing AlN wafers

Fig. 7 shows one of the free-standing, 1-inch diameter AlN wafers removed from its SiC substrate and then mounted on the seed holder for further homo-epitaxial growth. The SiC substrate has been removed by mechanical grinding from the backside using the diamond-embedded grinding plate. The as-grown surface is shown in the front view and there are no micro-pipes/holes in the prepared templates/wafers. Some of the cracks at the bottom are visible when looking through, since the wafer is transparent. Though there are few cracks at the backside, still the wafer is stable even after it was removed from its substrate and subsequent processing. Furthermore, cross-polariser images (not shown here) of the polished wafers show no difference in image-contrasts all over the surface, indicating the absence of mis-oriented grains. As presented in the above sections, AlN crystals grown in this study (either AlN/SiC templates or the free-standing wafers prepared from the templates) were shown to have better structural properties in comparison with other reported results of hetero-epitaxial growth and/or have comparable quality of homo-epitaxially grown crystals.

Thus for the technology development of large diameter AlN crystals, the epitaxial growth on foreign substrate approach is a very promising and potential way to achieve native AlN seeds with desired diameter when compared to another scaling approach of self-nucleation and homo seeding, wherein there are limitations in seed size, lateral enlargement, need of repetitive growth runs and each stage intermediate processing step to ultimately reach the desired size. Though unintentional, Si and C impurity incorporation in such a hetero-epitaxial growth is detrimental, these wafers are currently used as native seeds for the bulk single crystal growth in tungsten set-up (Si- and C-free environment), in which these impurities can be reduced to a greater extent.

4 Conclusions

In the presented work, a successful preparation of 28 mm diameter, crack-free, free-standing AlN wafers was achieved from hetero-epitaxially grown AlN crystals using SiC as a foreign substrate. X-ray rocking curves of the samples show FWHM values below 100 arcsec, with 100% of the wafer area being usable, without any polycrystalline inclusion/rim. Etch pit density is in the range of 2–5 $\times$ 10^5 cm^{-2}. Defect concentration and impurity incorporation along the whole wafer is very uniform as assessed by wet chemical etching, EPMA, Raman as well as CL measurements. This is very essential for obtaining homogeneous structural, optical as well as electrical properties across the wafer from the device fabrication point of view. These hetero-epitaxially grown AlN on SiC can be utilised as native substrates for further homo-epitaxial growth of structurally perfect and deep-UV transparent free-standing wafers by the PVT and/or HVPE methods. The scaling-up of this developed technology in order to meet the need for larger diameter AlN substrates is also possible.

Acknowledgements

The author is indebted to Prof. P. Gille for giving full freedom to work on this research topic, and also support throughout this project. This work was financially supported by the Bavarian Research Foundation through a research project (BFS – Nr. 860/09). The author would like to acknowledge gratefully the SiCrystal AG for providing good quality SiC substrates and also helping in the XRD measurements. The author also thanks Prof. M. Bickermann for his help and discussions during the CL measurements.

References

1 W. M. Yim, E. J. Stofko, P. J. Zanzucchi, J. I. Pankove, M. Ettenberg and S. L. Gilbert, *J. Appl. Phys.*, 1972, **44**, 292–296.
2 J. Li, K. B. Nam, M. L. Nakarmi, J. Y. Lin, H. X. Jiang, P. Carrier and S. H. Wei, *Appl. Phys. Lett.*, 2003, **83**, 5163–5165.
3 G. Yu, in *Properties of Advanced Semiconductor Materials GaN, AlN, InN, BN, SiC, SiGe*, ed. M. E. Levinshtein, S. L. Rumyantsev and M. S. Shur, Wiley, New York, 2001, pp. 31–47.
4 *Handbook of Nitride Semiconductors and Devices: Materials Properties, Physics and Growth*, ed. Hadis Morkoc, Wiley-VCH, 2008, vol. 1.
5 G. A. Slack, R. A. Tanzilli, R. O. Pohl and J. W. Vandersande, *J. Phys. Chem. Solids*, 1987, **48**, 641–647.
6 J. R. Grandusky, S. R. Gibb, M. C. Mendrick and L. J. Schowalter, *Appl. Phys. Express*, 2010, **3**, 072103.
7 H. Hirayama, S. Fujikawa, N. Noguchi, J. Norimatsu, T. Takano, K. Tsubaki and N. Kamata, *Phys. Status Solidi A*, 2009, **206**, 1176–1182.
8 A. Khan, S. Hwang and J. Lowder, *Proc. IEEE Int. Reliability Physics Symp.*, 2009, 89.

9 S. G. Mueller, R. T. Bondokov, K. E. Morgan, G. A. Slack, S. B. Schujman, J. Grandusky, J. A. Smart and L. J. Schowalter, *Phys. Status Solidi A*, 2009, **206**, 1153–1159.
10 M. Bickermann, B. M. Epelbaum, O. Filip, P. Heimann, S. Nagata and A. Winnacker, *Phys. Status Solidi*, 2010, **C7**, 21–24.
11 H. Helava, T. Chemekova, O. Avdeev, E. Mokhov, S. Nagalyuk, Y. Makarov and M. Ramm, *Phys. Status Solidi*, 2010, **C7**, 2115–2117.
12 M. Bickermann, B. M. Epelbaum, O. Filip, B. Tautz, P. Heimann and A. Winnacker, *Phys. Status Solidi*, 2012, **C9**, 449–452.
13 Y. Kumagai, Y. Kubota, T. Nagashima, T. Kinoshita, R. Dalmau, R. Schlesser, B. Moody, J. Xie, H. Murakami, A. Koukitu and Z. Sitar, *Appl. Phys. Express*, 2012, **5**, 055504.
14 N. Cabrera and D. A. Vermilyea, in *Growth and Perfection of Crystals*, ed. R. Doremus, B. Roberts and D. Turnbull, Wiley, New York, 1958, p. 393.
15 N. Ohtani, M. Katsuno, J. Takahashi, H. Yashiro and M. Kanaya, *Phys. Rev.*, 1999, **B59**, 4592–4595.
16 R. R. Sumathi, R. U. Barz, A. M. Gigler, T. Straubinger and P. Gille, *Phys. Status Solidi*, 2012, **A209**, 415–418.
17 P. Waltereit, C. Poblenz, S. Rajan, F. Wu, U. K. Mishra and J. S. Speck, *Jpn. J. Appl. Phys.*, 2004, **43**, L1520–L1523.
18 A. H. Ostadrahimi, H. Dabringhaus and K. Wandelt, *Surf. Sci.*, 2002, **521**, 139–150.
19 P. Lu, J. H. Edgar, C. Cao, K. Hohn, R. Dalmau, R. Schlesser and Z. Sitar, *J. Cryst. Growth*, 2008, **310**, 2464–2470.
20 M. Bickermann, O. Filip, B. M. Epelbaum, P. Heimann, M. Feneberg, B. Neuschl, K. Thonke, E. Wedler and A. Winnacker, *J. Cryst. Growth*, 2012, **339**, 13–21.
21 S. B. Schujman, L. J. Schowalter, R. T. Bondokov, K. E. Morgan, W. Liu, J. A. Smart and T. Bettles, *J. Cryst. Growth*, 2008, **310**, 887–890.
22 Z. G. Herro, D. Zhuang, R. Schlesser and Z. Sitar, *J. Cryst. Growth*, 2010, **312**, 2519–2521.
23 H. Kröncke, S. Figge, B. M. Epelbaum and D. Hommel, *Acta Phys. Pol.*, 2008, **A114**, 1193–1200.
24 *Properties of Silicon Carbide*, ed. G. L. Harris, Inspec/IEE, 1995, p.4.
25 V. Yu. Davydov, Yu. E. Kitaev, I. N. Goncharuk, A. N. Smirnov, J. Graul, O. Semchinova, D. Uffmann, M. B. Smirnov, A. P. Mirgorodsky and R. A. Evarestov, *Phys. Rev.*, 1998, **B58**, 12899–12907.
26 E. N. Mokhov, A. D. Roenkov, Yu. A. Vodakov, S. Yu. Karpov, M. S. Ramm, A. S. Segal, Yu. A. Makarov and H. Helava, *Mater. Sci. Forum*, 2003, **433–436**, 979–982.
27 J. A. Freitas, J. C. Culbertson, M. A. Mastro, Y. Kumagai and A. Koukitu, *J. Cryst. Growth*, 2012, **350**, 33–37.
28 M. Kuball, *Surf. Interface Anal.*, 2001, **31**, 987–999.
29 P. Perlin, J. Camassel, W. Knap, T. Taliercio, J. C. Chervin, T. Suski, I. Grzegory and S. Porowski, *Appl. Phys. Lett.*, 1995, **67**, 2524–2526.
30 R. R. Sumathi, R. U. Barz, T. Straubinger and P. Gille, *J. Cryst. Growth*, 2012, **360**, 193–196.
31 R. Dalmau, B. Moody, J. Xie, R. Collazo and Z. Sitar, *Phys. Status Solidi*, 2011, **A208**, 1545–1547.
32 G. A. Slack, L. J. Schowalter, D. Morelli and J. A. Freitas, *J. Cryst. Growth*, 2002, **246**, 287–298.
33 M. Bickermann, P. Heimann and B. M. Epelbaum, *Phys. Status Solidi*, 2006, **C3**, 1902–1906.
34 K. B. Nam, M. L. Nakarmi, J. Y. Lin and H. X. Jiang, *Appl. Phys. Lett.*, 2005, **86**, 222108.
35 N. Nepal, M. L. Nakarmi, J. Y. Lin and H. X. Jiang, *Appl. Phys. Lett.*, 2006, **89**, 092107.
36 T. Schulz, M. Albrecht, K. Irmscher, C. Hartmann, J. Wollweber and R. Fornari, *Phys. Status Solidi B*, 2011, **B248**, 1513–1518.
37 M. Strassburg, J. Senawiratne, N. Dietz, U. Haboeck, A. Hoffmann, V. Noveski, R. Dalmau, R. Schlesser and Z. Sitar, *J. Appl. Phys.*, 2004, **96**, 5870–5876.

